Supplementary Information

Green Synthesis of α-Aminophosphonates: From Hydrogen-Bonded Janus Dimers to Pharmaceutical Potential

Rawda Kholany,[a] Alaa A. Mardini,[b] Ksenia Shakirova,[a] Daut R. Islamov,[c] Alexander V. Gerasimov,[a] Alexander E. Klimovitskii,[a] Alena A. Vavilova,[a] Olga A. Mostovaya,[a] Asiya Gazizova,[a] Ivan I. Stoikov*[a]

[a] A.M. Butlerov Chemical Institute, Kazan Federal University, Kremlyovskaya, 18, 420008 Kazan, Russia;
[b] Damascus University, Faculty of Sciences, Chemistry Department, Damascus, Syrian Arab Republic
[c] Laboratory of Structural Analysis of Biomacromolecules, FRC Kazan Scientific Center of RAS, 31 Kremlevskaya Street, Kazan 420008, Russia
* Corresponding author. E-mail addresses: ivan.stoikov@mail.ru (I. Stoikov).

Contents

1. Materials and Methods

1.1. Chemicals

All reagents and solvents were obtained from Sigma-Aldrich and used without further purification, unless otherwise specified, in which case they were purified following established standard procedures.

1.2. Spectroscopic Characterization

Spectroscopic characterization was carried out using a range of analytical techniques. Nuclear magnetic resonance (NMR) spectroscopy was performed on a Bruker Avance 400 spectrometer (Bruker Corp., Billerica, MA, USA) operating at 400 MHz for ^{1}H nuclei and 162 MHz for ^{31}P nuclei, with ^{1}H and $^{31}P(H)$ NMR spectra acquired; samples were prepared as 3–5% solutions in $CDCl_3$, and residual solvent peaks served as the internal reference. Attenuated total reflectance Fourier-transform infrared (ATR-FTIR) spectroscopy was conducted using a Perkin Elmer Spectrum 400 spectrometer (Seer Green, UK) equipped with a diamond/KRS-5 accessory, with spectra collected at a resolution of 0.5 cm^{-1} over 64 scans (16 s acquisition time) within the 400–4000 cm^{-1} range. Ultraviolet-visible (UV-Vis) absorption measurements were performed on a Shimadzu UV-3600 spectrophotometer (Kyoto, Japan) using 10 mm quartz cuvettes, where samples were equilibrated for 1 h at 25 °C prior to analysis. Fluorescence emission spectra were obtained using a Horiba Fluorolog 3 spectrofluorometer (Longjumeau, France) with an excitation wavelength (λ_{ex}) of 270 nm and emission (λ_{em}) recorded between 280–500 nm, employing 5 nm slit widths and 10 mm quartz cuvettes; data were corrected using the instrument's software, and samples were incubated for 1 h at 298 K before measurement. High-resolution mass spectrometry (HRMS) data were acquired via electrospray ionization quadrupole time-of-flight (ESI-QTOF) mass spectrometry on a Bruker Impact II spectrometer (Bruker Daltonik GmbH, Germany), achieving a mass accuracy of ≤5 ppm. Single-crystal X-ray diffraction (SCXRD) data for the investigated compounds were collected using a Rigaku XtaLab Synergy S diffractometer equipped with a HyPix detector and a PhotonJet microfocus X-ray source operating with Cu Kα radiation (λ = 1.54184 Å) at low temperature. Data indexing and integration were performed with the CrysAlisPro software package. Systematic and absorption corrections were applied using the ABSPACK module, which employs numerical absorption correction via Gaussian integration over a multifaceted crystal model, as well as empirical absorption correction based on spherical harmonics according to the crystal's point group symmetry and equivalent reflections. The GRAL module was used to analyze systematic absences and determine the appropriate space group. Structural solutions were obtained by direct methods using SHELXT [1] and subsequent refinements were carried out by full-matrix least-squares refinement on F^2 using SHELXL [2]. Non-hydrogen atoms were refined anisotropically, while hydrogen atoms were positioned geometrically and refined using a riding model. Hydrogen atoms of methyl groups were located using a rotating group model with idealized tetrahedral geometry. Molecular graphics were generated using the Mercury 4.1 [3] program. Powder X-ray diffraction (PXRD) experiments were performed using a Rigaku MiniFlex 600 diffractometer (Rigaku, Tokyo, Japan) with a D/teX Ultra detector, operated at 30 kV and 15 mA, utilizing Cu K_α radiation (λ = 1.54178 Å) and a Ni filter to eliminate K_β radiation interference; data were acquired in continuous scan mode at a scanning rate of 5° per minute, and the resulting diffraction patterns were processed using the Expo2013 software package [4]. Thermal analysis was conducted via simultaneous thermogravimetry/differential scanning calorimetry (TG/DSC) on a Netzsch STA 449 C Jupiter thermoanalyzer (Germany) under an argon flow of 75 ml min^{-1} with a heating rate of 10 K min^{-1}; samples were equilibrated in air (2–3 min) and argon (18–20 min) at 25 °C prior to analysis, and clathrate guest content (S) was determined from TG curves with an error of ±0.05 mol guest/mol host. Dynamic light scattering (DLS) measurements for particle size was performed at 20 °C using a Malvern Zetasizer Nano ZS (4 mW He-Ne laser, λ = 633 nm, NIBS optics, 173° detection angle).

1.3. Computational details

All quantum chemical calculations were conducted using Spartan 20 (v1.1.4) [5] at the ωB97X-D/6-31G* level of theory, a hybrid range-separated density functional that incorporates empirical dispersion corrections [6]. This functional is particularly effective for describing non-covalent interactions such as hydrogen bonding, which is essential for modeling the geometry and electronic structure of dimeric systems stabilized by these interactions. [6, 7]. While ωB97X-D generally offers improved treatment of dispersion forces and long-range electron correlation compared to many other density functional theory (DFT) methods [8], vibrational frequencies obtained at this level are expected to be systematically higher than experimental values. This is primarily due to the harmonic approximation and the omission of environmental effects such as intermolecular interactions in the solid state [9-11]. Nevertheless, the method provides reliable relative trends and a solid theoretical framework for comparison with experimental spectra. Geometries were optimized in the gas phase, and the absence of imaginary vibrational frequencies confirmed that all structures correspond to true local minima on the potential energy surface. From the optimized geometries, a comprehensive set of reactivity descriptors, derived from frontier molecular orbital energies, was calculated, including the HOMO-LUMO energy gap (ΔE), chemical potential (μ)[12],

electronegativity (χ) [13], chemical hardness (η) [12], softness (S) [14], global electrophilicity index (ω), and electro-donating (ω^-) and electro-accepting (ω^+) powers [15], according to standard expressions (Equations 1–8). These descriptors were used to evaluate the electronic reactivity, thermodynamic stability, and potential biological activity of Compounds A, B, and C. Additionally, the application of Quantitative Structure–Activity Relationship (QSAR) analyses complemented the DFT results, allowing for the correlation of molecular electronic properties with bioactivity profiles [16]. The computational findings revealed significant variations in structural, electronic, and physicochemical characteristics among the compounds, emphasizing the suitability of the ωB97X-D/6-31G* level for capturing the nuanced behavior of molecular dimers and supporting its relevance in pharmaceutical modeling.

$$\Delta E_{gap} = E_{LUMO} - E_{HOMO} \quad (1)$$

$$\mu = -\frac{E_{HOMO}+E_{LUMO}}{2} \quad (2)$$

$$\chi = \frac{E_{HOMO}+E_{LUMO}}{2} \quad (3)$$

$$\eta = \frac{E_{LUMO}-E_{HOMO}}{2} \quad (4)$$

$$S = \frac{1}{2\eta} \quad (5)$$

$$\omega = \frac{\mu^2}{2\eta} \quad (6)$$

$$\omega^+ = \frac{(E_{LUMO}+3E_{HOMO})^2}{16(E_{LUMO}-E_{HOMO})} \quad (7)$$

$$\omega^- = \frac{(3E_{LUMO}+E_{HOMO})^2}{16(E_{LUMO}-E_{HOMO})} \quad (8)$$

2. Statistical Study

2.1. Statistical Equations [17]

Absolute Deviation (Δ)

$$\Delta = |\mathrm{Exp._i} - \mathrm{Calc._i}|$$

Percentage Deviation (Δ%):

$$\Delta\% = \left(\frac{|\mathrm{Exp._i} - \mathrm{Calc._i}|}{\mathrm{Exp._i}}\right) \times 100$$

Mean Absolute Error (MAE):

$$\mathrm{MAE} = \frac{1}{N}\sum_{i=1}^{N} |\mathrm{Exp._i} - \mathrm{Calc._i}|$$

Root Mean Square Error (RMSE):

$$\mathrm{RMSE} = \sqrt{\frac{1}{N}\sum_{i=1}^{N}(\mathrm{Exp._i} - \mathrm{Calc._i})^2}$$

2.2. Fourier-transform infrared spectroscopy (FT-IR)

Table S1 Experimental and calculated vibrational frequencies (cm^{-1}) of compounds A–C with deviations (Δ, Δ%), root mean square error (RMSE), and mean absolute error (MAE) for characteristic vibrational modes.

Vibrational Mode	Compound	Exp. (cm^{-1})	Calc. (cm^{-1})	Δ (cm^{-1})	Δ%	RMSE (cm^{-1})	MAE (cm^{-1})
Amine N-H Stretch	A	3338, 3269	3419, 3370	81, 101	2.43, 3.09	80.46	78
	B	3339, 3294	3418, 3355	79, 61	2.37, 1.85		
	C	3341, 3257	3387, 3357	46, 100	1.38, 3.07		
Amide N-H Stretch	A	3290, 3223	3410, 3335	120, 112	3.65, 3.48	90.90	87.33
	B	3216, 3172	3305, 3234	89, 62	2.77, 1.95		
	C	3289, 3212	3381, 3261	92, 49	2.80, 1.53		
Aromatic C-H Stretch	A	3100, 3046	3108, 3045	8, 1	0.26, 0.03	6.67	6.17
	B	3113	3108	5	0.16		

	C	3105, 3050, 3025	3113, 3057, 3033	8, 7, 8	0.26, 0.23, 0.26		
Aliphatic C-H Stretch	A	2994, 2975, 2950, 2850	2996, 2981, 2967, 2897	2, 6, 17, 47	0.07, 0.20, 0.58, 1.65	16.33	9.27
	B	2963, 2937, 2893, 2877	2963, 2937, 2895, 2885	0, 0, 2, 8	0.00, 0.00, 0.07, 0.28		
	C	2985, 2934, 2876	2985, 2932, 2894	0, 2, 18	0.00, 0.07, 0.63		
C=C Stretch	A	1605	1597	8	0.50	4.74	3.5
	B	1620	1615	5	0.31		
	C	1610, 1575	1610, 1574	0, 1	0.00, 0.06		
Amide C=O Stretch	A	1672	1720	48	2.87	41.92	41.67
	B	1664	1701	37	2.22		
	C	1669	1709	40	2.40		
P=O Stretch	A	1224	1226	2	0.16	7.62	5.33
	B	1206	1193	13	1.08		
	C	1215	1216	1	0.08		
P-O-C Stretch	A	1023, 1036	1024, 1038	1, 2	0.10, 0.19	3.81	3
	B	1059	1057	2	0.19		
	C	1010	1003	7	0.69		

2.3. Powder X-ray (XRPD) diffraction

Table S2 Experimental and calculated unit cell parameters of compounds A–C from XRPD, including deviations (Δ%), mean absolute error (MAE), and root mean square error (RMSE).

Parameter	Compound A (P $2_1/n$, Monoclinic)	Compound B (P -1, Triclinic)	Compound C (Pca 2_1, Orthorhombic)
a (Å)	Exp: 9.24880(10) / Calc: 9.24367 (Δ% = 0.06%)	Exp: 8.3755(4) / Calc: 8.38349 (Δ% = 0.10%)	Exp: 29.3313(6) / Calc: 29.2985 (Δ% = 0.11%)
b (Å)	Exp: 14.78870(10) / Calc: 14.78488 (Δ% = 0.03%)	Exp: 8.9060(3) / Calc: 8.90286 (Δ% = 0.04%)	Exp: 9.2370(2) / Calc: 9.29991 (Δ% = 0.68%)
c (Å)	Exp: 11.20740(10) / Calc: 11.19143 (Δ% = 0.14%)	Exp: 14.1032(5) / Calc: 14.10585 (Δ% = 0.02%)	Exp: 14.2141(4) / Calc: 14.16233 (Δ% = 0.36%)
Angles (°)	β: Exp: 95.8870(10) / Calc: 95.7219 (Δ% = 0.17%)	α,β,γ: <0.14% deviation (γ max Δ% = 0.14%)	α=β=γ=90° (perfect match)
Volume ($Å^3$)	Exp: 1524.84 / Calc: 1521.87 (Δ% = 0.19%)	Exp: 982.441 / Calc: 982.838 (Δ% = 0.04%)	Exp: 3851.07 / Calc: 3858.86 (Δ% = 0.20%)
Crystallite Size (nm)	46.09	58.69	60.94
MAE	0.0083 Å (a,b,c), 0.17° (β)	0.0046 Å (a,b,c), 0.14° (γ)	0.049 Å (a,b,c)
RMSE	0.0099 Å, 0.17° (β)	0.0052 Å, 0.14° (γ)	0.0507 Å

2.4. Proton Nuclear magnetic resonance spectroscopy (^{1}H NMR)

Table S3 Experimental and calculated ^{1}H NMR chemical shifts (ppm) for different proton groups in Compounds A–C, along with the deviations (Δ, Δ%), squared deviations ($Δ^2$), and corresponding statistical error metrics (RMSE and MAE).

Proton Group	Compound A					Compound B					Compound C					RMSE	MAE
	(Exp.)	(Calc.)	(Δ)	(Δ%)	$(Δ)^2$	(Exp.)	(Calc.)	(Δ)	(Δ%)	$(Δ)^2$	(Exp.)	(Calc.)	(Δ)	(Δ%)	$(Δ)^2$		
$C(CH_3)_2$	1.31	1.52	0.21	16.03	0.044	1.32	1.50	0.18	13.64	0.03	1.44	1.18	0.26	18.06	0.07	0.22	0.22
$NCOCH_3$	2.00	1.74	0.26	13.00	0.068	1.99	1.89	0.10	5.03	0.01	2.14	2.10	0.04	1.87	0.00	0.16	0.13
C–NH–C	2.02	2.41	0.39	19.31	0.152	2.01	2.67	0.66	32.84	0.44	–	1.79	–	–	–	0.54	0.53
NH–CO	6.96	6.10	0.86	12.36	0.740	7.55	9.12	1.57	20.79	2.46	7.80	8.24	0.44	5.64	0.19	1.06	0.96
Aromatic	6.81	6.83	0.02	0.29	0.000	6.79	7.06	0.27	3.98	0.07	6.99	6.52	0.47	6.72	0.22	0.31	0.25
OCH_3 / OCH_2 / OCH	3.59	3.98	0.39	10.86%	0.152	3.82	3.75	0.07	1.83	0.00	4.67	4.67	0.00	0.00	0.00	0.23	0.15
C–C–CH_3	–	–	–	–	–	0.75	0.85	0.10	13.33	0.01	–	–	–	–	–	0.10	0.10
C–CH_2–C	–	–	–	–	–	1.48	1.70	0.22	14.86	0.05	–	–	–	–	–	0.22	0.22
C–CH_3(a)	–	–	–	–	–	–	–	–	–	–	1.24	1.50	0.26	20.97	0.07	0.26	0.26

2.5. Ultraviolet–visible spectroscopy (UV-Vis)

Table S4 Experimental and calculated UV–Vis absorption (λ_{max}, FWHM) and emission data for Compounds A–C in H_2O:EtOH (9.25:0.25), including deviations (Δ, Δ%, Δ^2) for absorption bands and corresponding Stokes shifts from experimental emission maxima.

Compound	Absorption						Emission		
	(Exp.), λ_{max} (nm)	FWHM (nm)	(Calc.), λ_{max} (nm)	Δ	Δ%	$(\Delta)^2$	(Exp.), λ_{max} (nm)	FWHM (nm)	Stokes Shift ($\Delta\lambda$, nm)
A	197.40	17.67	190.00	7.40	3.75	54.76	-	-	-
	254.80	37.27	238.00	16.80	6.59	282.24	364.00	63.50	109.20
B	197.80	16.90	192.00	5.80	2.93	33.64	-	-	-
	255.00	35.51	230.00	25.00	9.80	625.00	365.50	61.93	110.50
C	198.20	17.31	182.00	16.20	8.17	262.44	-	-	-
	254.80	36.19	226.00	28.80	11.30	829.44	365.50	61.31	110.70

Table S5 Statistical error analysis of calculated versus experimental UV–Vis transition bands, showing cumulative deviations ($\sum\Delta$, $\sum\Delta^2$) along with mean absolute error (MAE) and root mean square error (RMSE) for high- and low-energy absorptions.

Transition Band	$\sum\Delta$	$\sum(\Delta)^2$	MAE (nm)	RMSE (nm)
High-energy	29.40	350.84	9.80	10.8
Low-energy	70.60	1736.68	23.5	24.1

3. Tables and figures

3.1. Single-crystal X-ray diffraction

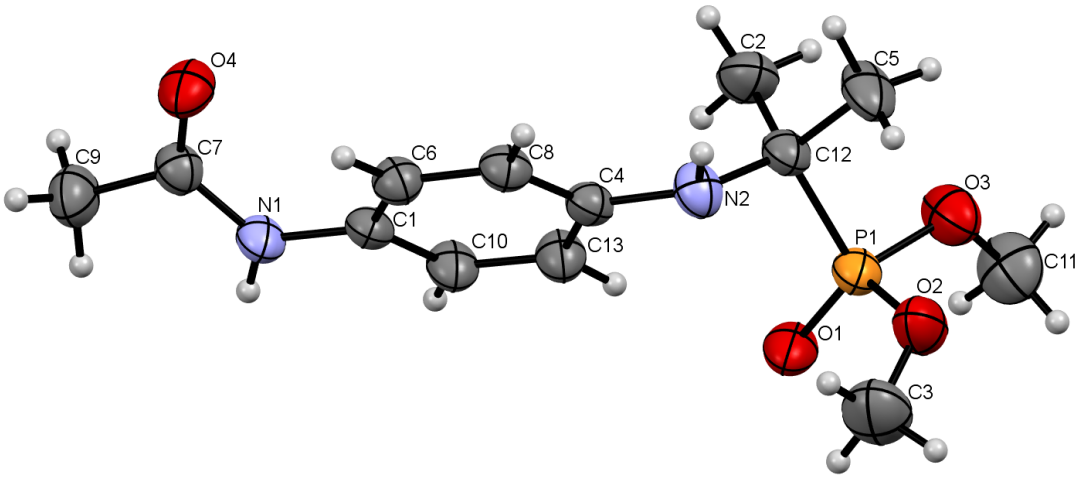

Figure S 1 ORTEP representation of Compound **A** showing 50% probability thermal ellipsoids. C atoms –grey, N atoms – blue, O atoms – red, P atoms – orange.

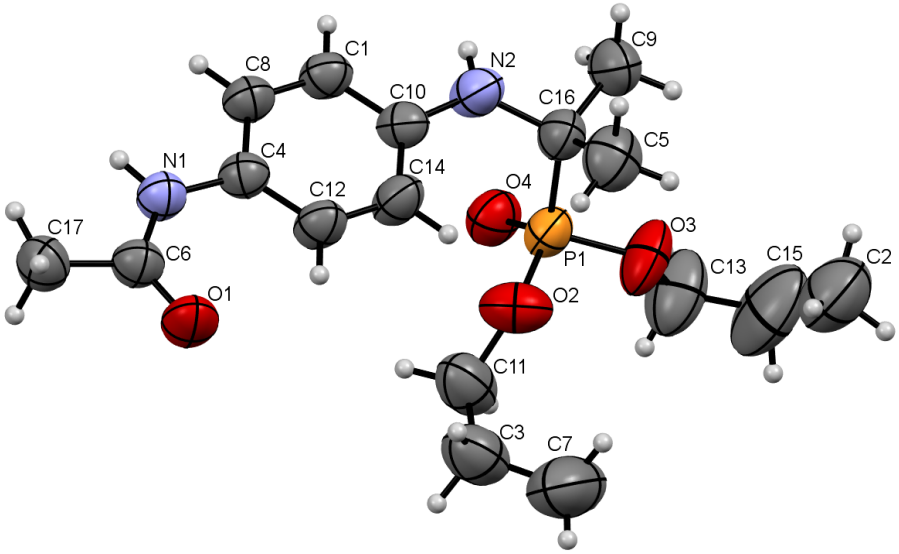

Figure S 2 ORTEP representation of Compound **B** showing 50% probability thermal ellipsoids. Disordered atoms have been omitted for clarity. C atoms –grey, N atoms – blue, O atoms – red, P atoms – orange.

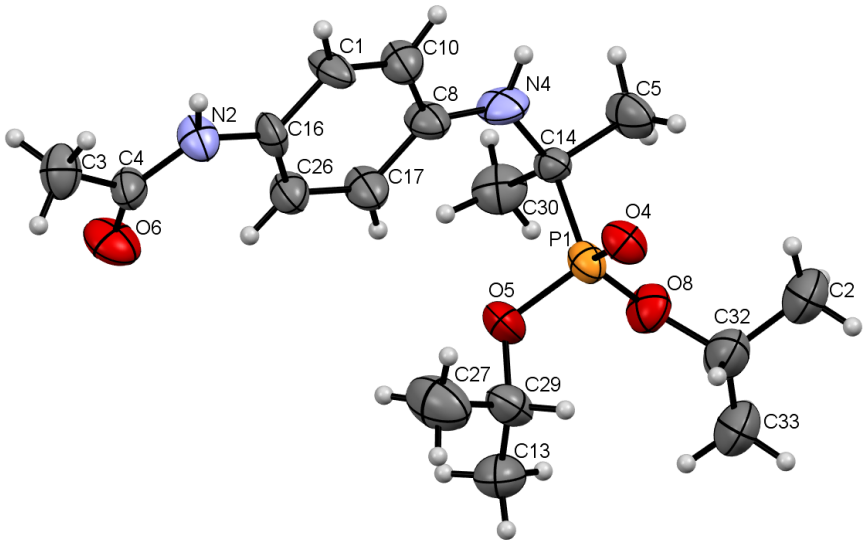

Figure S 3 ORTEP representation of Compound **C** showing 50% probability thermal ellipsoids. Disordered atoms have been omitted for clarity. C atoms –grey, N atoms – blue, O atoms – red, P atoms – orange.

Table S6 Crystal data and structure refinement for A, B and C.

Compound	A	B	C
Empirical formula	$C_{13}H_{21}N_2O_4P$	$C_{17}H_{29}N_2O_4P$	$C_{17}H_{29}N_2O_4P$
Formula weight	300.29	356.39	356.39
Temperature/K	304.06(10)	303.8(9)	304.7(5)
Crystal system	monoclinic	triclinic	orthorhombic
Space group	$P2_1/n$	P-1	$Pca2_1$
a/Å	9.24880(10)	8.3755(4)	29.3313(6)
b/Å	14.78870(10)	8.9060(3)	9.2370(2)
c/Å	11.20740(10)	14.1032(5)	14.2141(4)
α/°	90	79.245(3)	90
β/°	95.8870(10)	82.358(3)	90
γ/°	90	72.517(4)	90
Volume/Å^3	1524.84(2)	982.44(7)	3851.07(16)
Z	4	2	8
ρ_{calc} mg/mm^3	1.308	1.205	1.229
μ/mm^{-1}	1.738	1.423	1.452
F(000)	640.0	384.0	1536.0
Crystal size/mm^3	0.382 × 0.270 × 0.206	0.395 × 0.083 × 0.022	0.218 × 0.142 × 0.105
2Θ range for data collection	9.936 to 152.072°	10.542 to 152.532°	6.026 to 151.894°
Index ranges	-11 ≤ h ≤ 11, -18 ≤ k ≤ 18, -14 ≤ l ≤ 13	-10 ≤ h ≤ 10, -10 ≤ k ≤ 11, -17 ≤ l ≤ 17	-36 ≤ h ≤ 36, -11 ≤ k ≤ 8, -17 ≤ l ≤ 17
Reflections collected	20745	24581	44008
Independent reflections	3142[R^{18} = 0.0372]	3885[R^{18} = 0.0557]	7886[R^{18} = 0.0470]
Data/restraints/parameters	3142/0/194	3885/1/235	7886/38/440
Goodness-of-fit on F^2	1.126	1.524	2.459
Final R indexes [I>=2σ (I)]	R_1 = 0.0464, wR_2 = 0.1216	R_1 = 0.1057, wR_2 = 0.3349	R_1 = 0.2583, wR_2 = 0.4849
Final R indexes [all data]	R_1 = 0.0484, wR_2 = 0.1239	R_1 = 0.1116, wR_2 = 0.3411	R_1 = 0.2606, wR_2 = 0.4896
Largest diff. peak/hole / e Å^{-3}	0.34/-0.58	0.98/-0.41	7.02/-0.76
CCDC Refcode	2496614	2496616	2496615

Table S7 Comparison of experimental and calculated (DFT-wB97X-D/6-31G*) bond lengths (Å) for compound **A**.

	A-B	Bond Length (Å)		|Δ|		A-B	Bond Length (Å)		|Δ|
		Exp.	Calc.				Exp.	Calc.	
1	C9-C7	1.503	1.518	0.015	11	C4-N2	1.414	1.407	0.007
2	C7-N1	1.349	1.367	0.018	12	N2-C12	1.478	1.455	0.023
3	C7-O4	1.221	1.219	0.002	13	C12-C2	1.531	1.54	0.009
4	N1-C1	1.415	1.403	0.012	14	C12-C5	1.538	1.537	0.001
5	C1-C6	1.392	1.397	0.005	15	C12-P1	1.831	1.861	0.03
6	C6-C8	1.383	1.387	0.004	16	P1-O1	1.468	1.483	0.015
7	C8-C4	1.392	1.402	0.01	17	P1-O2	1.564	1.611	0.047
8	C4-C13	1.398	1.398	0	18	P1-O3	1.573	1.621	0.048
9	C13-C10	1.384	1.389	0.005	19	O2-C3	1.416	1.438	0.022
10	C10-C1	1.388	1.395	0.007	20	O3-C11	1.418	1.427	0.009

Table S8 Comparison of experimental and calculated (DFT-wB97X-D/6-31G*) bond lengths (Å) for compound **B**.

	A-B	Bond Length (Å)		|Δ|		A-B	Bond Length (Å)		|Δ|
		Exp.	Calc.				Exp.	Calc.	
1	C17-C6	1.49	1.519	0.029	13	C16-C5	1.53	1.53	0
2	C6-O1	1.237	1.222	0.015	14	C16-C9	1.542	1.538	0.004
3	C6-N1	1.345	1.368	0.023	15	C16-P1	1.846	1.859	0.013
4	N1-C4	1.408	1.406	0.002	16	P1-O4	1.456	1.49	0.034
5	C4-C12	1.384	1.399	0.015	17	P1-O2	1.561	1.608	0.047
6	C12-C14	1.385	1.393	0.008	18	O2-C11	1.45	1.432	0.018
7	C14-C10	1.392	1.394	0.002	19	C11-C3	1.478	1.519	0.041
8	C10-C1	1.389	1.397	0.008	20	C3-C7	1.461	1.527	0.066
9	C1-C8	1.372	1.384	0.012	21	P1-O3	1.561	1.606	0.045
10	C8-C4	1.395	1.401	0.006	22	C13-O3	1.398	1.448	0.05
11	C10-N2	1.386	1.428	0.042	23	C13-C15	1.431	1.514	0.083
12	N2-C16	1.457	1.474	0.017	24	C15-C2	1.402	1.529	0.127

Table S9 Comparison of experimental and calculated (DFT-wB97X-D/6-31G*) bond lengths (Å) for compound **C**.

	A-B	Bond Length (Å)		|Δ|		A-B	Bond Length (Å)		|Δ|
		Exp.	Calc.				Exp.	Calc.	
1	C3-C4	1.442	1.516	0.074	13	C14-C5	1.512	1.532	0.02
2	C4-O6	1.281	1.223	0.058	14	C14-C30	1.502	1.538	0.036
3	C4-N2	1.361	1.369	0.008	15	C14-P1	1.861	1.85	0.011
4	N2-C16	1.351	1.408	0.057	16	P1-O4	1.491	1.486	0.005
5	C16-C1	1.411	1.398	0.013	17	P1-O8	1.5489	1.608	0.0591
6	C1-C10	1.382	1.389	0.007	18	P1-O5	1.581	1.603	0.022
7	C10-C8	1.392	1.398	0.006	19	O8-C32	1.512	1.452	0.06
8	C8-C17	1.382	1.398	0.016	20	C32-C33	1.522	1.521	0.001
9	C17-C26	1.412	1.39	0.022	21	C32-C2	1.542	1.521	0.021
10	C26-C16	1.382	1.399	0.017	22	O5-C29	1.452	1.447	0.005
11	C8-N4	1.411	1.416	0.005	23	C29-C27	1.463	1.519	0.056
12	N4-C14	1.452	1.464	0.012	24	C29-C13	1.492	1.52	0.028

Table S 10: Comparison of experimental SC-XRD bond lengths with ωB97X-D/6-31G optimized geometries for Compounds A–C with deviations (Δ, Δ%), root mean square error (RMSE), and mean absolute error (MAE).

Bond	Compound	Exp. (A°)	Calc. (A°)	Δ (A°)	Δ%	RMSE (cm^{-1})	MAE (cm^{-1})
C-N	**A**	1.349, 1.415, 1.414, 1.478	1.367, 1.403, 1.407, 1.455	0.018, 0.012, 0.007, 0.023	1.33, 0.85, 0.50, 1.56	0.02	0.02
	B	1.345, 1.408, 1.386, 1.457	1.368, 1.406, 1.428, 1.474	0.023, 0.002, 0.042, 0.017	1.71, 0.14, 3.00, 1.17		
	C	1.361, 1.351, 1.411, 1.452	1.369, 1.408, 1.416, 1.464	0.008, 0.057, 0.005, 0.012	0.59, 4.22, 0.40, 0.83		
C=O	**A**	1.221	1.219	0.002	0.16	0.03	0.03
	B	1.237	1.222	0.015	1.21		
	C	1.281	1.223	0.058	4.53		
P-O	**A**	1.564, 1.573	1.611, 1.621	0.047, 0.048	3.01, 3.05	0.05	0.04
	B	1.561, 1.561	1.608, 1.606	0.047, 0.045	3.01, 2.88		
	C	1.5489, 1.581	1.608, 1.603	0.059, 0.022	3.82, 1.39		
C=C	**A**	1.392, 1.383, 1.392, 1.398, 1.384, 1.388	1.397, 1.387, 1.402, 1.398, 1.389, 1.395	0.005, 0.004, 0.010, 0.000, 0.005, 0.007	0.36, 0.29, 0.72, 0.00, 0.36, 0.50	0.01	0.01
	B	1.384, 1.385, 1.392,	1.399, 1.393, 1.394,	0.015, 0.008, 0.002,	1.08, 0.58, 0.14,		

		1.389, 1.372, 1.395	1.397, 1.384, 1.401	0.008, 0.012, 0.006	0.58, 0.87, 0.43		
	C	1.411, 1.382, 1.392, 1.382, 1.412, 1.382	1.398, 1.389, 1.398, 1.398, 1.39, 1.399	0.013, 0.007, 0.006, 0.016, 0.022, 0.017	0.92, 0.51, 0.43, 1.16, 1.56, 1.23		
P=O	**A**	1.468	1.483	0.015	1.02	0.02	0.02
	B	1.456	1.49	0.034	2.34		
	C	1.491	1.486	0.005	0.34		
C-P	**A**	1.831	1.861	0.03	1.64	0.02	0.02
	B	1.846	1.859	0.013	0.70		
	C	1.861	1.85	0.011	0.59		

Table S11 Comparison of experimental and calculated (DFT-wB97X-D/6-31G*) bond angles (°) for compound **A**.

	A-B-C	Angle (°)		|Δ|		A-B-C	Angle (°)		|Δ|
		Exp.	Calc.				Exp.	Calc.	
1	C9-C7-O4	121.5	121.68	0.18	12	N2-C12-C2	113.91	106.12	7.79
2	C9-C7-N1	114.71	113.65	1.06	13	N2-C12-C5	106.81	112.15	5.34
3	C7-N1-C1	126.41	127.2	0.79	14	C5-C12-C2	109.21	108.36	0.85
4	N1-C1-C10	118.71	117.47	1.24	15	N2-C12-P1	109.11	116.36	7.25
5	N1-C1-C6	123.01	124.23	1.22	16	C12-P1-O1	116.538	114.2	2.338
6	C1-C10-C13	121.42	121.48	0.06	17	C12-P1-O3	100.968	108.59	7.622
7	C10-C13-C4	120.52	120.71	0.19	18	C12-P1-O2	106.958	102.52	4.438
8	C13-C4-C8	117.61	117.21	0.4	19	O1-P1-O3	115.218	112.54	2.678
9	C4-C8-C6	121.81	122.3	0.49	20	O1-P1-O2	113.528	110.18	3.348
10	C8-C6-C1	120.21	119.79	0.42	21	P1-O3-C11	123.11	118.38	4.73
11	C4-N2-C12	123.11	127.48	4.37	22	P1-O2-C3	123.02	124.52	1.5

Table S12 Comparison of experimental and calculated (DFT-wB97X-D/6-31G*) bond angles (°) for compound **B**.

	A-B-C	Angle (°)		|Δ|		A-B-C	Angle (°)		|Δ|
		Exp.	Calc.				Exp.	Calc.	
1	C17-C6-O1	121.93	121.46	0.47	13	N2-C16-C9	105.43	106.61	1.18
2	C17-C6-N1	114.93	114	0.93	14	C16-P1-O4	115.22	111.14	4.08
3	C6-N1-C4	130.33	127.66	2.67	15	C16-P1-O3	102.72	102.39	0.33
4	N1-C4-C12	124.93	124.31	0.62	16	C16-P1-O2	105.12	114.36	9.24
5	N1-C4-C8	117.13	116.78	0.35	17	O4-P1-O3	114.32	116.57	2.25
6	C4-C8-C1	120.73	120.82	0.09	18	O4-P1-O2	114.42	107.54	6.88
7	C8-C1-C10	122.33	120.6	1.73	19	P1-O3-C13	125.64	117.4	8.24
8	C1-C10-C14	116.53	118.25	1.72	20	O3-C13-C15	111.76	108.93	2.83
9	C10-C14-C12	122.03	121.56	0.47	21	C13-C15-C2	113.31	110.4	2.91
10	C14-C12-C4	120.63	119.5	1.13	22	P1-O2-C11	124.23	127.7	3.47
11	C10-N2-C16	130.03	117.82	12.21	23	O2-C11-C3	108.25	108.17	0.08
12	N2-C16-C5	113.23	112.17	1.06	24	C11-C3-C7	112.26	111.33	0.93

Table S13 Comparison of experimental and calculated (DFT-wB97X-D/6-31G*) bond angles (°) for compound **C**.

	A-B-C	Angle (°)		|Δ|		A-B-C	Angle (°)		|Δ|
		Exp.	Calc.				Exp.	Calc.	
1	C3-C4-O6	121.1	121.22	0.12	13	N4-C14-C30	113.1	112.63	0.47
2	C3-C4-N2	120.1	118.63	1.47	14	C14-P1-O4	116.26	114.82	1.44
3	C4-N2-C16	135.1	130.77	4.33	15	C14-P1-O8	104.95	103.11	1.84
4	N2-C16-C1	117.1	118.1	1	16	C14-P1-O5	104.76	105.83	1.07
5	C16-C1-C10	119.1	120.43	1.33	17	O4-P1-O8	112.05	116.68	2.02
6	C1-C10-C8	124.1	121.23	2.87	18	O4-P1-O5	113.96	110.03	3.93
7	C10-C8-C17	116.1	118.09	1.99	19	P1-O8-C32	124.17	125.55	1.38
8	C8-C17-C26	122.1	120.92	1.18	20	P1-O5-C29	120.1	128.74	8.64
9	C17-C26-C16	121.1	120.65	0.45	21	O8-C32-C33	109.1	112.02	2.92
10	C26-C16-C1	118.1	118.58	0.48	22	O8-C32-C2	104.1	110.47	6.37
11	C8-N4-C14	132.1	122.96	9.14	23	O5-C29-C13	110.1	106.43	3.67
12	N4-C14-C5	106.1	111.35	5.25	24	O5-C29-C27	109.1	108.43	0.67

Table S 14 Comparison of experimental SC-XRD Angles (°) with ωB97X-D/6-31G optimized geometries for Compounds **A–C** with deviations (Δ, Δ%), root mean square error (RMSE), and mean absolute error (MAE).

Angle	Compound	Exp. (°)	Calc. (°)	Δ (°)	Δ%	RMSE (°)	MAE (°)
C-N-C	**A**	126.41, 123.11	127.2, 127.48	0.79, 4.37	0.62, 3.55	6.81	5.59
	B	130.33, 130.03	127.66, 117.82	2.67, 12.21	2.05, 9.39		
	C	135.1, 132.1	130.77, 122.96	4.33, 9.14	3.21, 6.92		
O=P-C	**A**	116.538	114.2	2.34	2.01	2.84	2.62
	B	115.22	111.14	4.08	3.54		
	C	116.26	114.82	1.44	1.24		
C-P-O	**A**	100.968, 106.958	108.59, 102.52	7.62, 4.44	7.55, 4.15	5.29	4.09
	B	102.72, 105.12	102.39, 114.36	0.33, 9.24	0.32, 8.79		
	C	104.95, 104.76	103.11, 105.83	1.84, 1.07	1.75, 1.02		
C=C-C (aromatic ring)	**A**	121.42, 120.52, 117.61, 121.81, 120.21	121.48, 120.71, 117.21, 122.3, 19.79	0.06, 0.19, 0.4, 0.49, 0.42	0.05, 0.16, 0.34, 0.40, 0.35	1.26	0.97
	B	120.73, 122.33, 116.53, 122.03, 120.63	120.82, 120.6, 118.25, 121.56, 119.50	0.09, 1.73, 1.72, 0.47, 1.13	0.07, 1.41, 1.48, 0.39, 0.94		
	C	1119.1, 124.1, 116.1, 122.1, 121.1	120.43, 121.23, 118.09, 120.92, 120.65	1.33, 2.87, 1.99, 1.18, 0.45	1.12, 2.31, 1.71, 0.97, 0.37		

O-P=O	**A**	115.218, 113.528	112.54, 110.18	2.68, 3.35	2.32, 2.95	4.24	3.95
	B	114.32, 114.42	116.57, 107.54	2.25, 6.88	1.97, 6.01		
	C	112.05, 113.96	116.68, 110.03	4.63, 3.93	4.13, 3.45		

3.2. ATR analysis

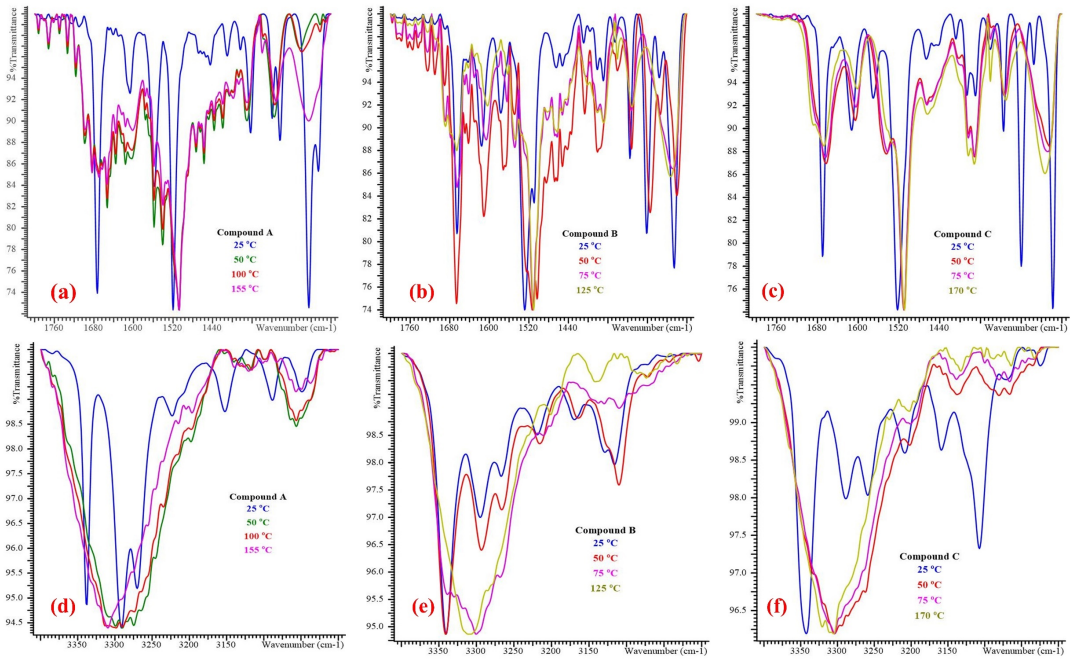

Fig. S4 ATR spectral analysis of compounds A, B, and C: (a–c) 1200–1800 cm^{-1} region and (d–f) 3000–3400 cm^{-1} region.

Table S15 Frequencies of compounds **A**, **B**, and **C** in the crystal phase and under thermal heating (50–170 °C).

Compound	T ° C	$\bar{\upsilon}\ cm^{-1}$				
		N-H stretching amine	N-H stretching amide	C=O	N-H bending	P=O
A	Crystal	3338 3269	3290 3223	1672	1520	1224
	50	Broad peak 3274		1653 1669 1683	1507	-
	100	Broad peak 3289		1653 1669 1684	1507	-
	155	Broad peak 3309		1654 1669 1684	1507	1244
B	Crystal	3339 3294	3216 3172	1664	1528	1206

	50	3340 3293	3266 3215	1666	1524	1220
	75	Broad peak 3295		1665 1678	1511	1226
	125	Broad peak 3306		1667 1680	1511	1232
C	Crystal	3341 3257	3289 3212	1669	1522	1215
	50	Broad peak 3304		1662	1510	1224
	75	Broad peak 3304		1663	1509	1227
	170	Broad peak 3305		1667 1688	1509	1232

3.3. High-resolution mass spectrometry (HRMS)

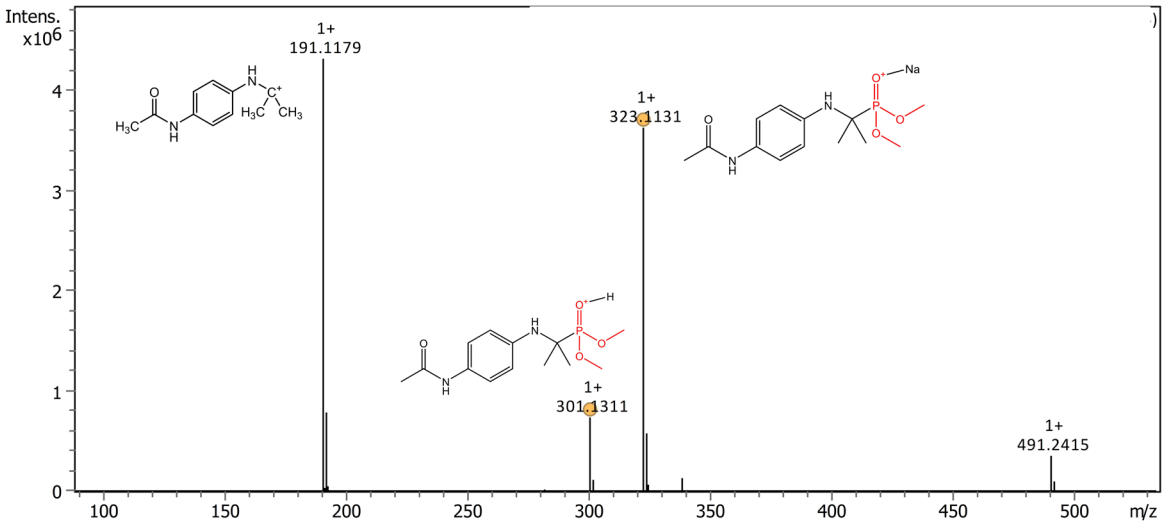

Fig. S5 High-resolution mass spectrometry (HRMS) analysis of compound A.

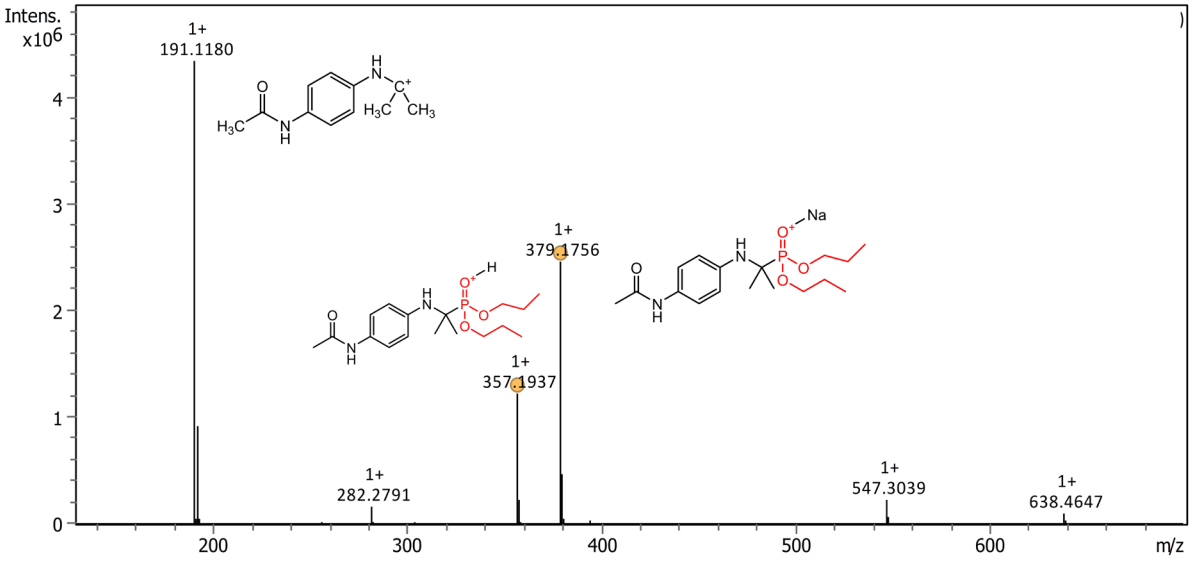

Fig. S6 High-resolution mass spectrometry (HRMS) analysis of compound B.

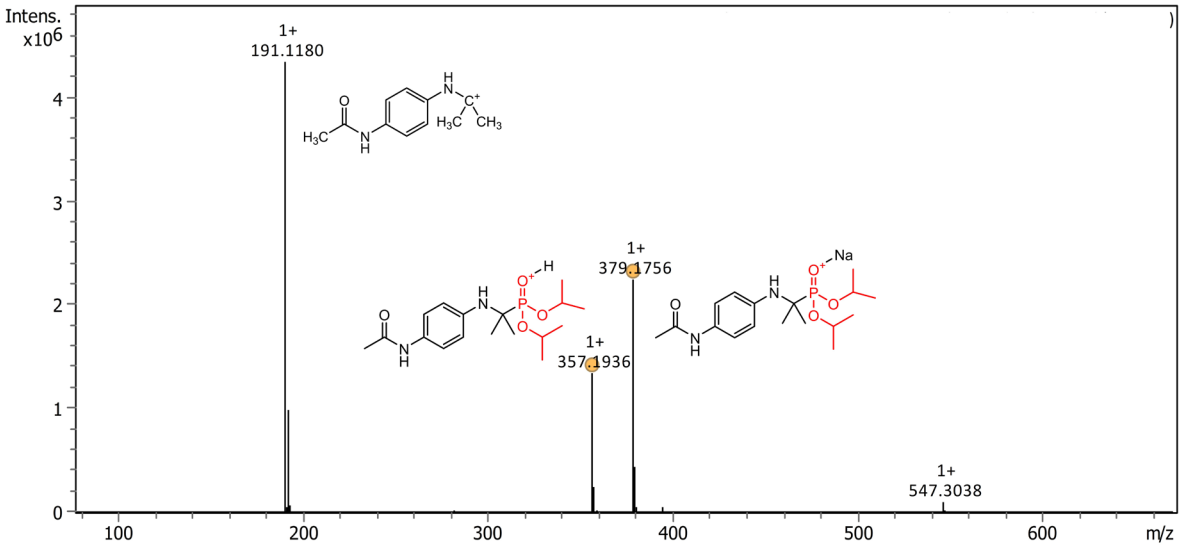

Fig. S7 High-resolution mass spectrometry (HRMS) analysis of compound C.

3.4. Nuclear magnetic resonance spectroscopy NMR

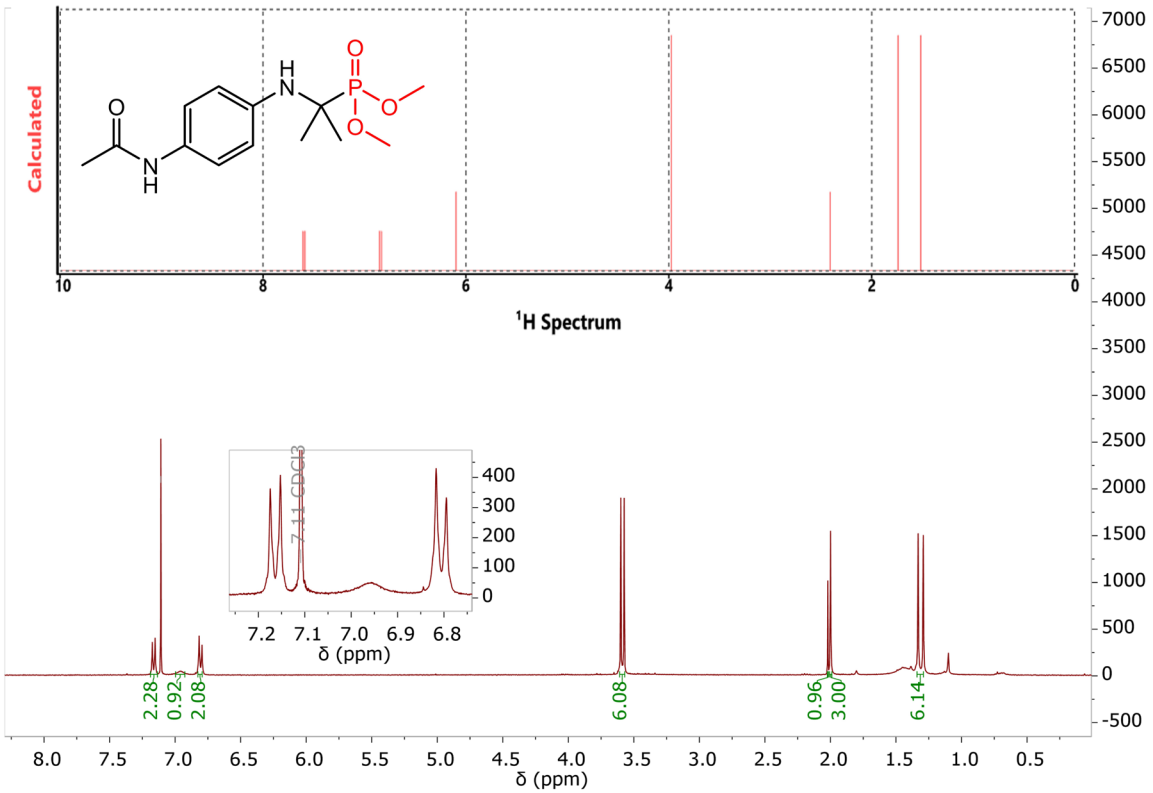

Fig. S8 ^{1}H NMR spectrum of compound A. Theoretical spectrum calculated in the gas phase (as a dimer) compared with the experimental spectrum recorded in $CDCl_3$.

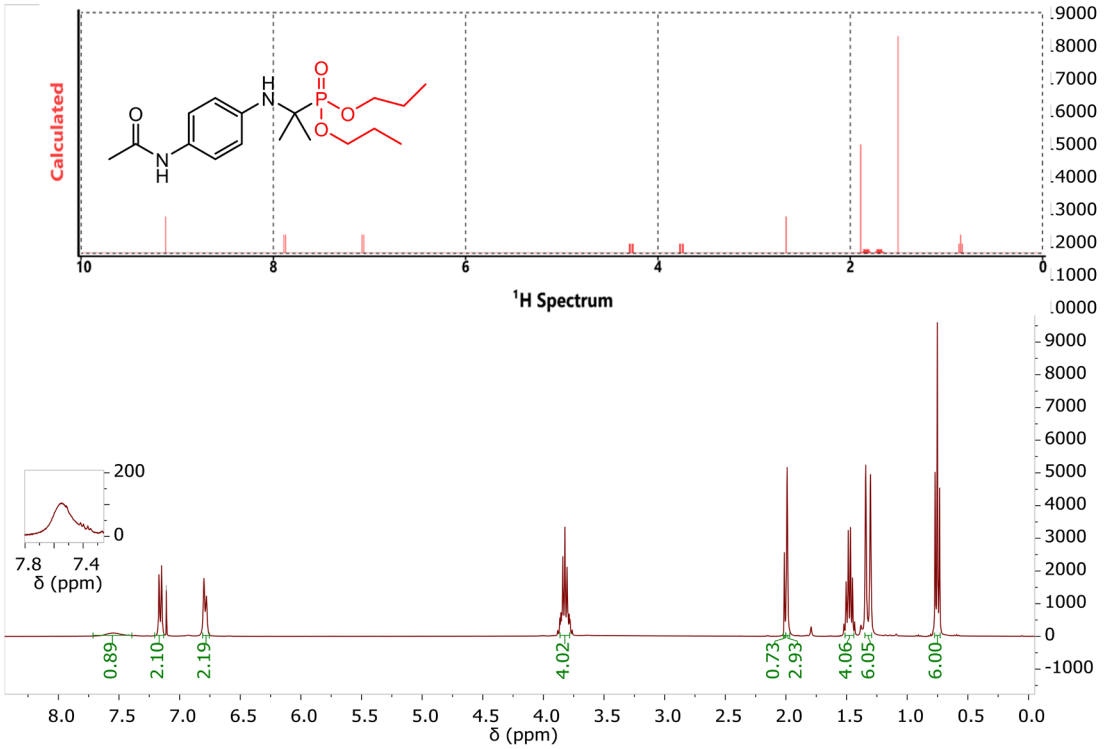

Fig. S9 ^{1}H NMR spectrum of compound B. Theoretical spectrum calculated in the gas phase (as a dimer) compared with the experimental spectrum recorded in $CDCl_3$.

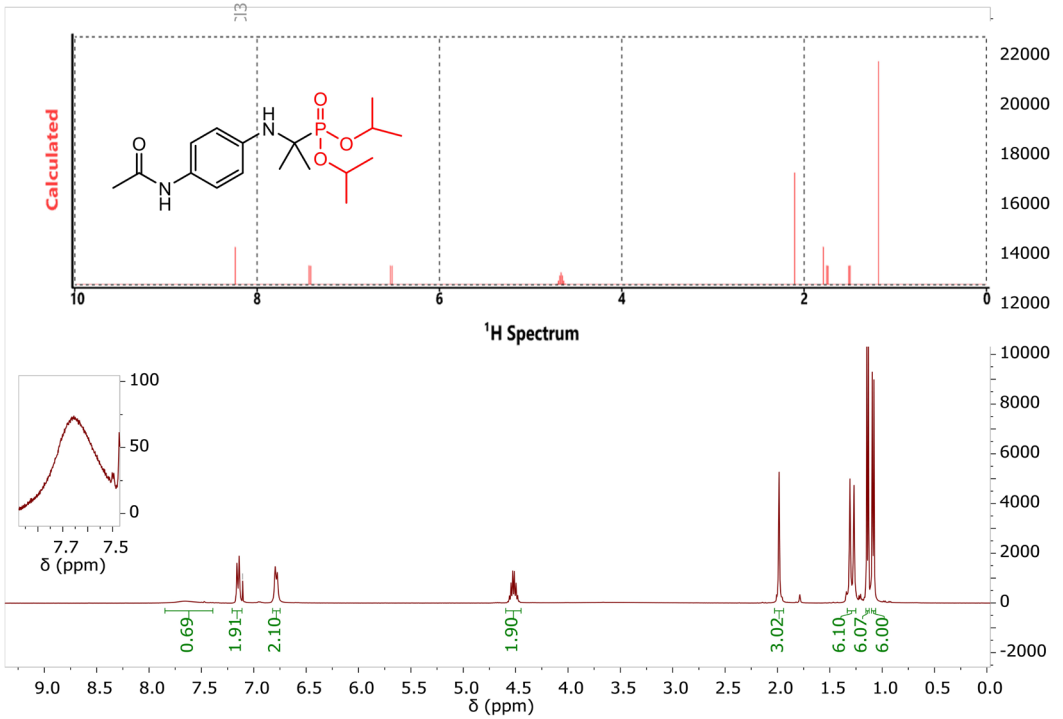

Fig. S10 ^{1}H NMR spectrum of compound C. Theoretical spectrum calculated in the gas phase (as a dimer) compared with the experimental spectrum recorded in $CDCl_3$

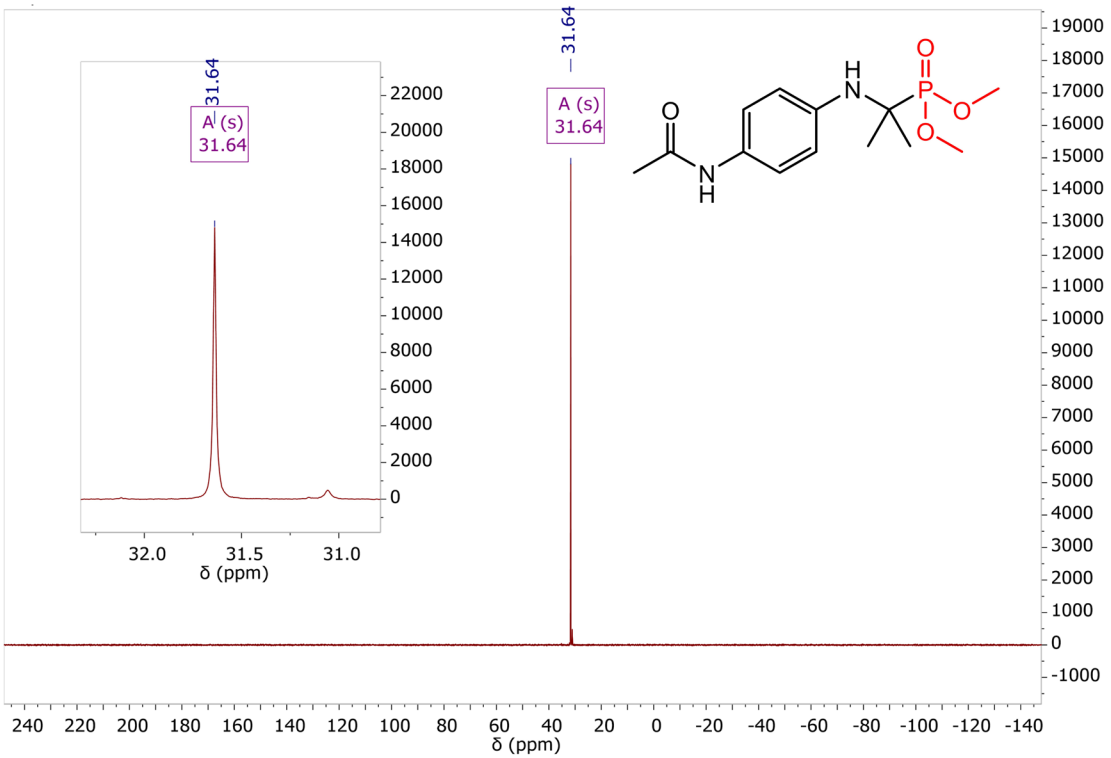

Fig. S11 ^{31}P(H) NMR of the compound A in $CDCl_3$.

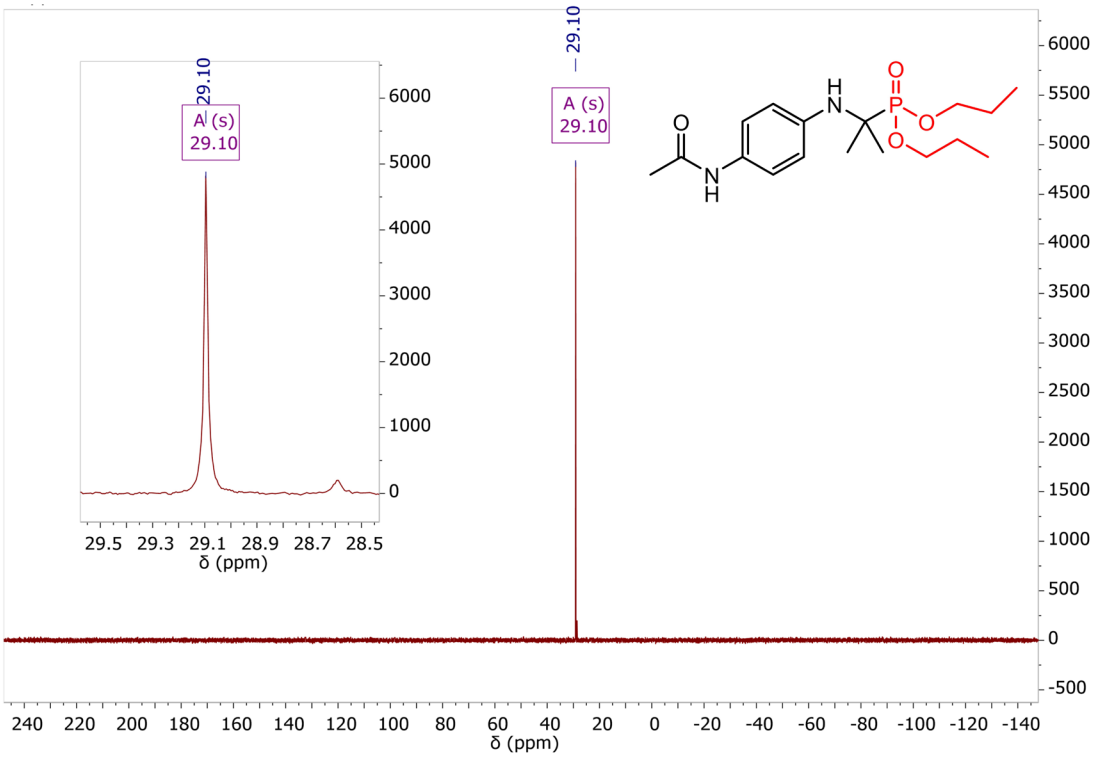

Fig. S12 ^{31}P(H) NMR of the compound B in $CDCl_3$.

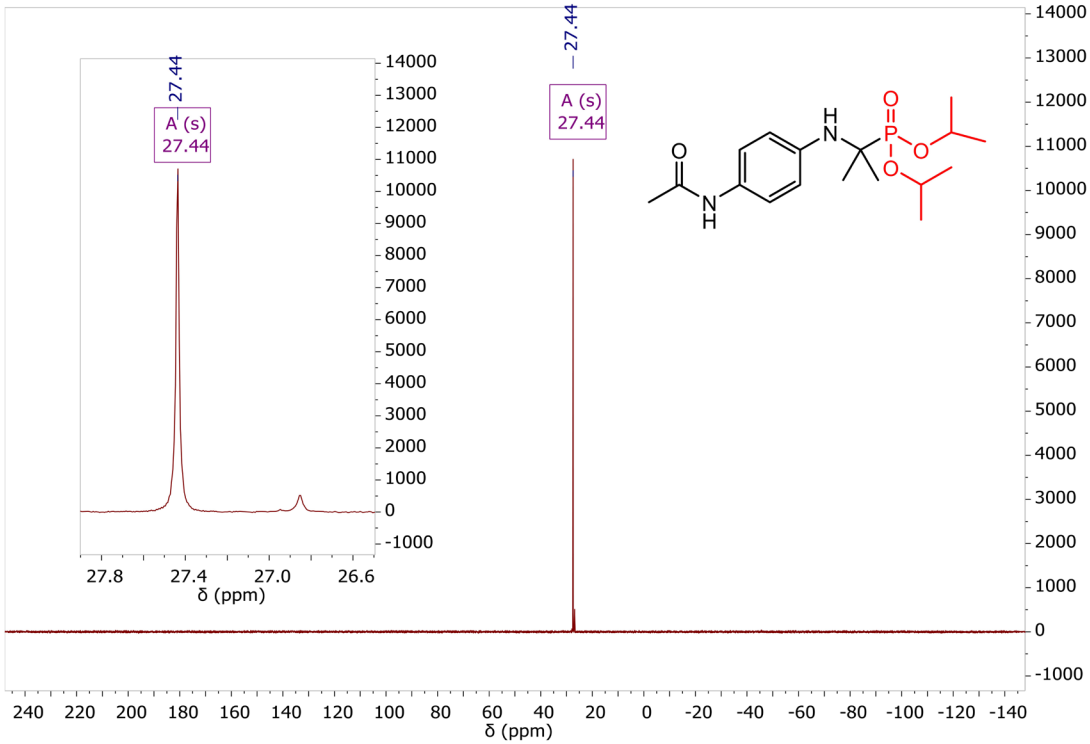

Fig. S13 ^{31}P(H) NMR of the compound C in $CDCl_3$.

3.5. ^{1}H NMR and FT-IR Analysis of Dimeric Compounds

Table S16 Experimental (in $CDCl_3$) and calculated (gas phase, monomer and dimer) chemical shifts (δ, ppm) of protons for compounds A, B, and C.

Chemical shift δ (ppm)											
Compound A				Compound B				Compound C			
Proton Group	Exp	Calc. Mon.	Calc. Dim.	Proton Group	Exp	Calc. Mon.	Calc. Dim.	Proton Group	Exp	Calc. Mon.	Calc. Dim.
$\mathbf{C(CH_3)_2}$	1.31	1.53	1.52	$C(CH_3)_2$	1.32	1.58	1.50	$C(CH_3)_2$	1.44	1.21	1.18
$\mathbf{NCOCH_3}$	2.00	1.58	1.74	$NCOCH_3$	1.99	1.88	1.89	$NCOCH_3$	2.14	1.93	2.10
C-NH-C	2.02	3.45	2.41	C-NH-C	2.01	3.34	2.67	C-NH-C	-	2.88	1.79
NH-CO	6.96	5.29	6.10	NH-CO	7.55	5.46	9.12	NH-CO	7.80	5.62	8.24
Aromatic ring	6.81 7.16	6.50 7.02	6.83 7.59	Aromatic ring	6.79 7.16	6.51 7.38	7.06 7.87	Aromatic ring	6.99 7.30	6.98 7.46	6.52 7.41
$\mathbf{OCH_3}$	3.59	3.95	3.98	OCH_2	3.82	4.33 4.09	3.75 4.27	OCH	4.67	4.74	4.67
–	-		-	$C-C$ $-CH_3$	0.75	1.28	0.85	C $-CH_3(a)$ C $-CH_3(b)$	1.24 1.29	1.54 1.60	1.5 1.79
–	-		-	$C-CH_2$ $-C$	1.48	1.48 2.07	1.7 1.83	-	-		-

Table S17 Experimental (solid state) and calculated (gas phase, monomer and dimer) vibrational frequencies of compounds A, B, and C.

	Vibrational frequencies ($\mathbf{cm^{-1}}$)								
	Compound A			Compound B			Compound C		
	Exp.	Calc. Mon	Calc. Dim	Exp.	Calc. Mon	Calc. Dim	Exp.	Calc. Mon	Calc. Dim
$\nu_{(N-H)}$ amine	3338 3269	3415	3419 3370	3339 3294	3423	3418 3355	3341 3257	3347	3387 3357
$\nu_{(N-H)}$ amide	3290 3223	3421	3410 3335	3216 3172	3455	3305 3234	3289 3212	3456	3381 3261
$\nu_{(C-H)}$ aromatic	3100 3046	3101 3048	3108 3045	3113	3019	3108	3105 3050 3025	3106 3016	3113 3057 3033
$\nu_{(C-H)}$ aliphatic	2994 2975 2950 2850	3003 2996 2909 2901	2996 2981 2967 2897	2963 2937 2893 2877	2979 2990 2989 2980	2963 2937 2895 2885	2985 2934 2876	2988 2921 2898	2985 2932 2894
$\nu_{(C=O)}$ amide	1672	1734	1720	1664	1725	1701	1669	1732	1709
$\nu_{(C=C)}$	1605	1613	1597	1620	1622	1615	1610 1575	1613 1585	1610 1574
$\nu_{(N-H)}$ bending	1520	1572	1550	1528	1489	1497	1522 1475	1589 1512	1525 1465
$\nu_{(C-N)}$	1302 1243	1353 1307	1301 1266	1278	1262	1269	1103 1137	1203 1182	1118 1120
$\nu_{(P=O)}$	1224	1228	1226	1206	1222	1193	1215	1207	1216
$\nu_{(P-O-C)}$	1023 1036	1043 1062	1024 1038	1059	1060	1057	1010	988	1003

3.6. Photophysical properties (UV-Vis and Fluorescence)

Table S18 Experimental absorption and emission wavelengths (nm) of compounds A, B, and C in a water-ethanol mixture (9.25:0.25, v/v), along with TD-DFT-calculated absorption wavelengths (gas phase, wB97X-D/6-31G* level of theory).

Compound	Absorption				Experimental Emission		$\Delta\lambda = \lambda_{em} - \lambda_{abs}$
	Experimental		Calculated				
	λ_{max} (nm)	FWHM (nm)	λ_{max} (nm)	MO contributions	λ_{max} (nm)	FWHM (nm)	
Compound A	197.4	17.67	190	H-5→L (18%) H-3→L (17%)	-	-	-
	254.8	37.27	238	H-1→L (78%)	364	63.5	109.2
Compound B	197.8	16.90	192	H-2→L+1 (38%) H-5→L+3 (16%)	-	-	-
	255	35.51	230	H-1→L+2 (70%)	365.5	61.93	110.5
Compound C	198.2	17.31	182	H-2→L (50%)	-	-	-
	254.8	36.19	226	H-5→L+2 (31%) H→L+2 (13%)	365.5	61.31	110.7

3.7. Dynamic Light Scattering DLS

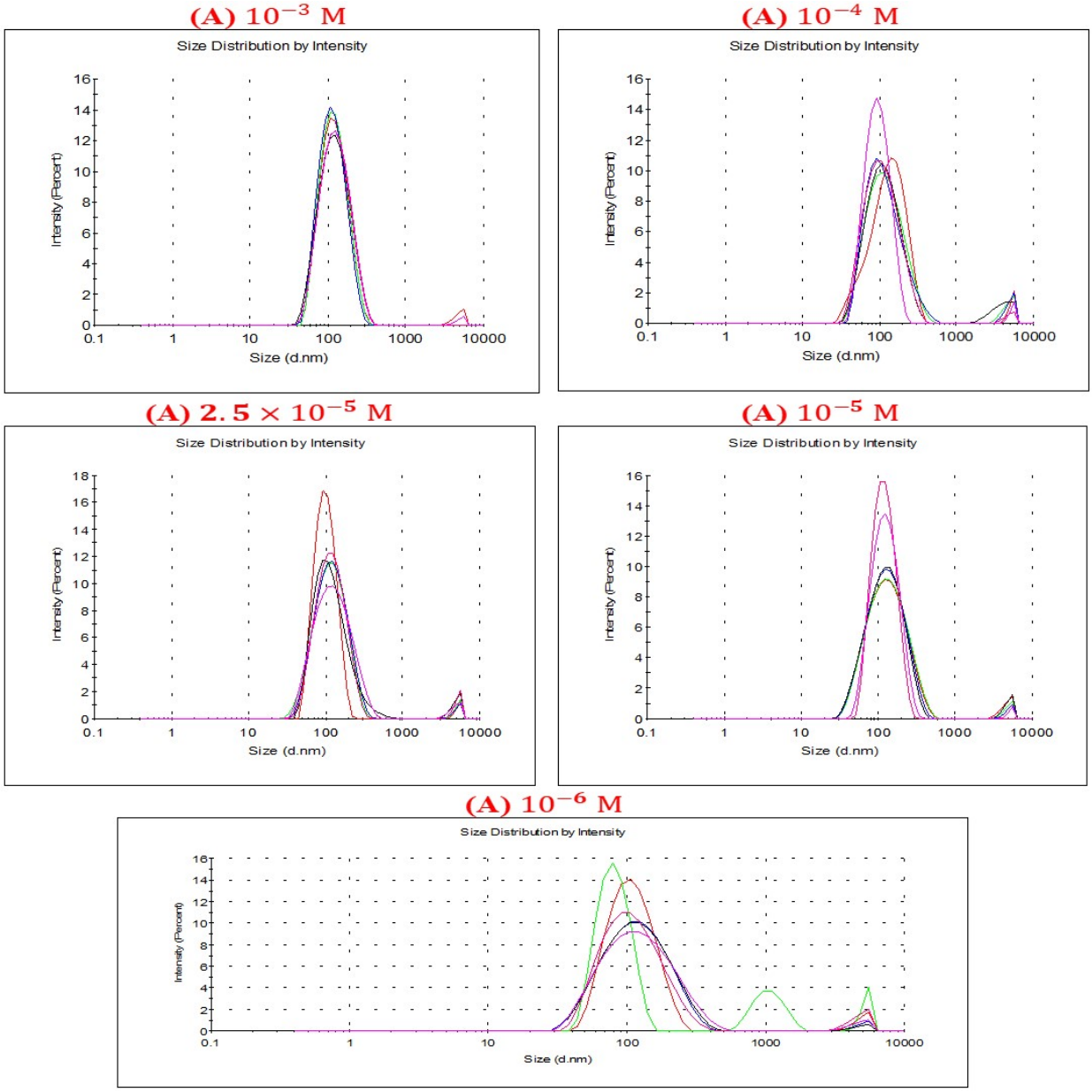

Fig. S14 Size distributions of Compound A measured by dynamic light scattering (DLS) in a water-ethanol (8:2, v/v) mixture.

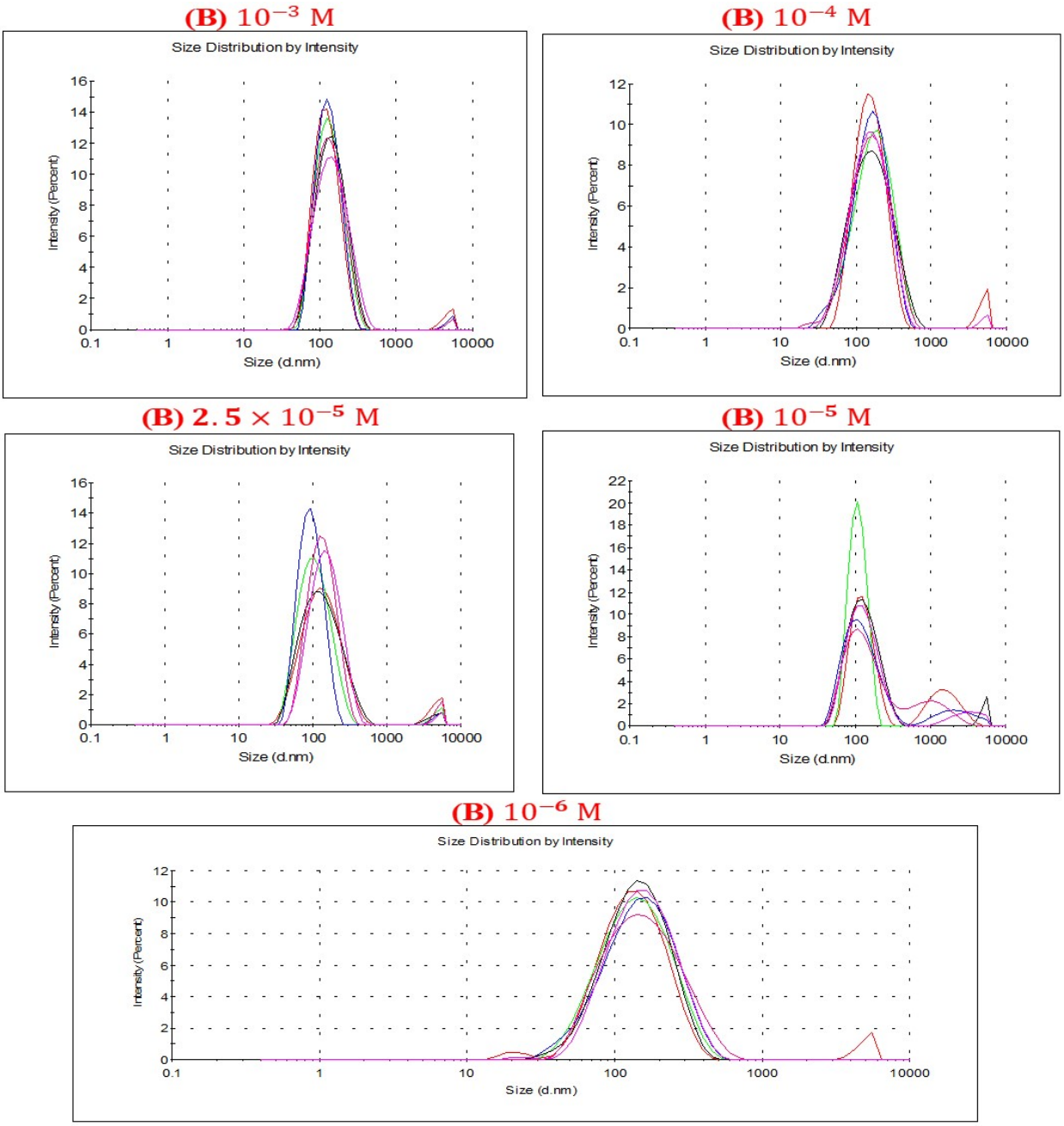

Fig. S15 Size distributions of Compound B measured by dynamic light scattering (DLS) in a water-ethanol (8:2, v/v) mixture.

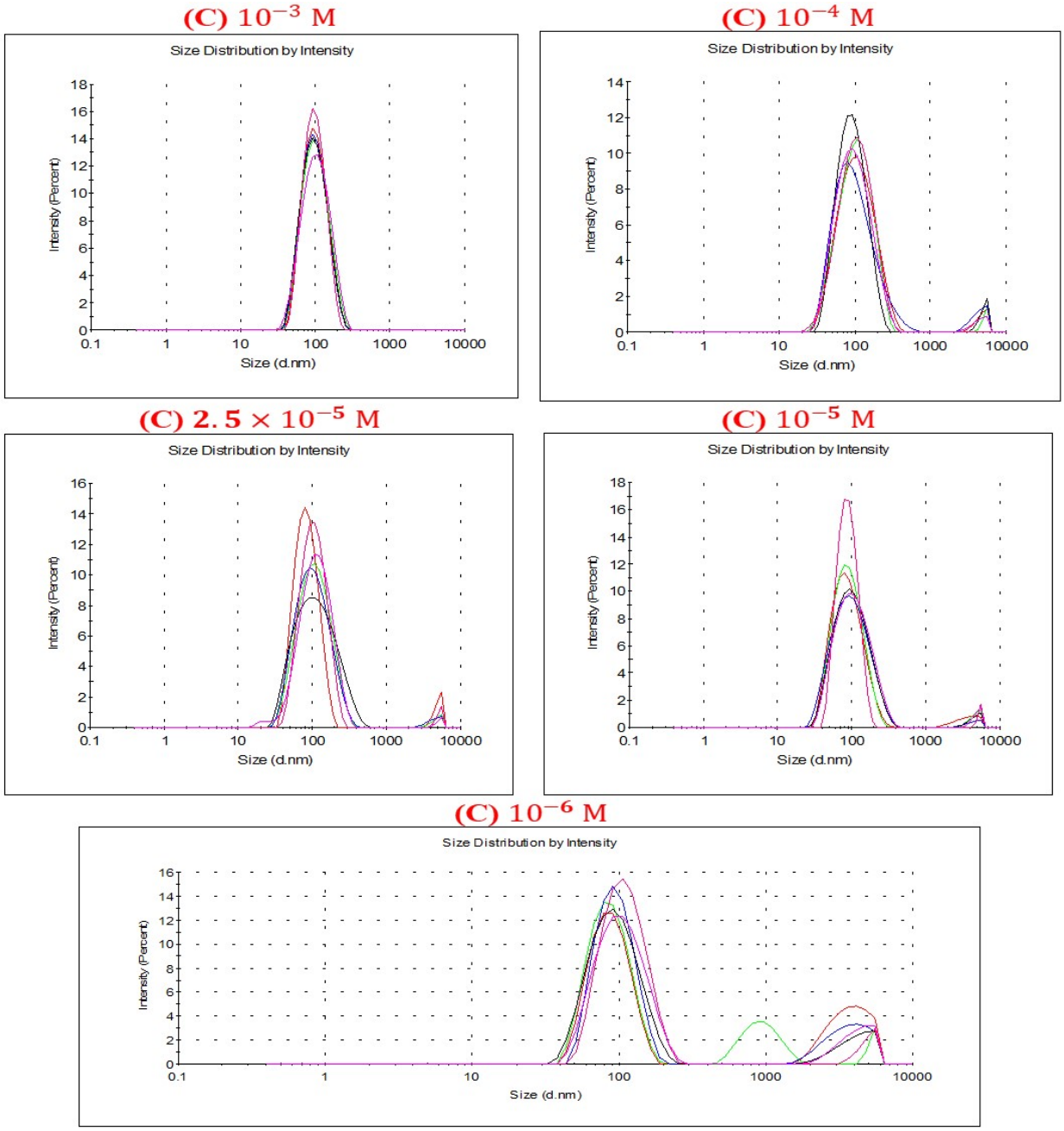

Fig. S16 Size distributions of Compound C measured by dynamic light scattering (DLS) in a water-ethanol (8:2, v/v) mixture.

3.8. Thermal analysis (TG/DSC)

Table S19 Thermal analysis data (TG, DSC, and DTG) of compounds A, B, and C.

Property/Feature	Compound A (Dimethyl)	Compound B (Dipropyl)	Compound C (Diisopropyl)
Melting Point (°C)	151.1	124.5	160.7
1st Endothermic Peak (°C)	151.1 (+86.66 J/g)	124.5 (+100.1 J/g)	160.7 (+117.9 J/g)
2nd Endothermic Peak (°C)	-	185.4 (+120.5 J/g)	200.6 (+112.6 J/g)
Moisture/Volatile Loss (%)	−0.01	−0.64	0.00
Number of Decomp. Steps	5	6	4
DTG Peaks (°C)	170.3, 288.0, 317.5, 441.0	206.2, 310.4, 453.3	212.1, 322.2

3.9. DFT Calculations

Table S20 Calculated electronic structure parameters for compounds A, B, and C in the gas phase, including energy gap (ΔE_{gap}), chemical potential (μ), electronegativity (χ), chemical hardness (η), chemical softness (S), global electrophilicity index (ω), electro-accepting power (ω+), and electro-donating power (ω−).

	Compound A (Dimer)	Compound B (Dimer)	Compound C (Dimer)
E_{HOMO} (eV)	-6.7	-7.2	-7.2
E_{LUMO} (eV)	1.9	1.8	1.6
ΔE_{gap} (eV)	8.6	9	8.8
μ (eV)	2.4	2.7	2.8
χ (eV)	-2.4	-2.7	-2.8
η (eV)	4.3	4.5	4.4
S (eV^{-1})	0.116	0.111	0.114
ω (eV)	0.669	0.810	0.891
ω^+ (eV)	2.407	2.722	2.841
ω^- (eV)	0.0072	0.0225	0.0409
Dipole Moment (D)	12.08	14.05	9.30

Table S21 Quantitative Structure-Activity Relationship (QSAR) Analysis of Compounds A, B, and C.

QSAR		A	B	C
Space-filling (CPK) model	Surface area of a space-filling (CPK) model Å^2	614.32	773.49	762.74
	Volume of a space-filling (CPK) model Å^3	600.10	745.16	745.65
	Polar surface area of a space-filling (CPK) model (PSA) Å^2	110.453	107.050	104.495
	CPK Ovality	1.79	1.95	1.92
From Computed Electron Density	Accessible Area Å^2	301.09	367.82	354.11
	Minimum value of the electrostatic potential (Min ElPot) KJ/mol	-244.51	-224.70	-218.21
	Maximum value of the electrostatic potential (Max ElPot) KJ/mol	191.42	221.77	94.85
	Polar Area (75) Å^2	202.20	164.87	115.99
	Accessible Polar Area (75) Å^2	126.61	84.37	53.81
	Accessible Non-Polar Area (75) Å^2	174.48	283.45	300.30
	Minimum value of the local ionization potential Min LocIonPot (eV)	10.35	9.92	9.66
Number of hydrogen-bond donor sites (HBD)		4	4	4
Number of hydrogen-bond acceptor sites (HBA)		12	12	12
Polarizability		88.05	99.72	99.78

References

1. G. M. Sheldrick, *Acta Crystallogr., Sect. A: Found. Adv*, 2014, 70, C1437.
2. G. M. Sheldrick, *Foundations of crystallography*, 2008, 64, 112–122.
3. C. F. Macrae, P. R. Edgington, P. McCabe, E. Pidcock, G. P. Shields, R. Taylor, M. Towler and J. Streek, *Applied Crystallography*, 2006, 39, 453–457.
4. A. Altomare, C. Cuocci, C. Giacovazzo, A. Moliterni, R. Rizzi, N. Corriero and A. Falcicchio, *Applied Crystallography*, 2013, 46, 1231–1235.
5. *Journal*, 2020.
6. J.-D. Chai and M. Head-Gordon, *Physical Chemistry Chemical Physics*, 2008, 10, 6615–6620.
7. G. A. DiLabio and A. Otero-de-la-Roza, *Reviews in computational chemistry*, 2016, 29, 1–97.
8. K. S. Thanthiriwatte, E. G. Hohenstein, L. A. Burns and C. D. Sherrill, *Journal of Chemical Theory and Computation*, 2011, 7, 88–96.
9. J. J. Panek and A. Jezierska, *Journal of Molecular Modeling*, 2015, 21, 15.
10. R. L. Jacobsen, R. D. Johnson III, K. K. Irikura and R. N. Kacker, *Journal of Chemical Theory and Computation*, 2013, 9, 951–954.
11. P. Popelier, A. Lenstra, C. Van Alsenoy and H. Geise, *Structural Chemistry*, 1991, 2, 3–9.
12. A. A. Mardini, I. A. Shuklov, A. A. Lizunova and V. F. Razumov, *Nano-Structures & Nano-Objects*, 2024, 39.
13. C.-G. Zhan, J. A. Nichols and D. A. Dixon, *The Journal of Physical Chemistry A*, 2003, 107, 4184–4195.
14. B. Kosar and C. Albayrak, *Spectrochimica Acta Part A: Molecular and Biomolecular Spectroscopy*, 2011, 78, 160–167.
15. H. Roohi and N. Mohtamadifar, *RSC advances*, 2022, 12, 11557–11573.
16. S. Van Damme and P. Bultinck, *Journal of Computational Chemistry*, 2009, 30, 1749–1757.
17. Y. Dodge, *The concise encyclopedia of statistics*, Springer Science & Business Media, 2008.
18. G. Keglevich and E. Bálint, *Molecules*, 2012, 17, 12821–12835.